Extraction of boron nitride nanotubes and fabrication of macroscopic articles using chlorosulfonic acid

Mohammed Adnan,[1,†] Daniel M. Marincel,[1] Olga Kleinerman,[2] Sang-Hyon Chu,[3] Cheol Park,[4] Samuel Hocker,[4] Catharine Fay,[4] Sivaram Arepalli,[1] Yeshayahu Talmon,[2] and Matteo Pasquali[1,‡]

[1]Department of Chemical and Biomolecular Engineering and Department of Chemistry, The Smalley-Curl Institute, Rice University, Houston, TX 77005, USA.

[2]Department of Chemical Engineering, Technion-Israel Institute of Technology and the Russell Berrie Nanotechnology Institute (RBNI), Haifa 3200003, Israel.

[3]National Institute of Aerospace, 100 Exploration Way, Hampton, VA 23666, USA.

[4]NASA Langley Research Center, Hampton, VA 23681, USA

Nanotechnology; Boron nitride nanotubes; Chlorosulfonic acid; Nanotube extraction; Thin films; Foams

Due to recent advances in high-throughput synthesis, research on boron nitride nanotubes (BNNTs) is moving towards applications. One future goal is the assembly of macroscopic articles of high aspect ratio, pristine BNNTs. However, these articles are presently unattainable because of insufficient purification and fabrication methods. We introduce a solution process for extracting

1

BNNTs from synthesis impurities without sonication or the use of surfactants and proceed to convert the extracted BNNTs into thin films. The solution process can also be used to convert as-synthesized material—which contains significant amounts of hexagonal boron nitride (h-BN)—into mats and foams with controllable structure and dimension. The scalable solution extraction method, combined with further advances in synthesis and purification, contributes to the development of all-BNNT macroscopic articles, such as fibers and 3-D structures.

Boron nitride nanotubes (BNNTs) are structural analogues of carbon nanotubes (CNTs) with comparable Young's modulus (1.3 TPa), tensile strength (~40 GPa),[1] and thermal conductivity (300-3000 W/mK).[2] BNNTs are chemically different from CNTs; they are wide bandgap semiconductors regardless of chirality[3] and are stable up to 900°C in air.[4] In addition, BNNTs are piezoelectric[5] and photoluminescent in the ultraviolet range.[6] Due to these unique properties, BNNTs are being targeted for use in applications such as oxidation resistant heat shields,[7, 8] chemically inert catalyst supports, high-temperature dielectrics for electrical wires, and chemical resistant coatings for metals.[9]

The development of gram-scale synthesis in the laboratory setting has prepared BNNTs to be useful in a variety of applications. Starting with the first synthesis in 1995,[10] BNNTs have primarily been synthesized using low-throughput synthesis techniques, permitting selectivity for high concentrations of crystalline BNNTs with few byproducts but at the expense of a low production rate.[11] The past decade has seen the development of several routes to produce gram-scale quantities of BNNTs, including the high temperature-pressure (HTP) method[12] and the radio frequency induction plasma based synthesis with and without hydrogen.[13, 14] All the high production methods rely on high-temperature condensation and growth that results in higher material production rates with significant synthesis byproducts, including boron nitride polymorphs like hexagonal boron nitride (h-BN).

Several purification routes have been developed[15-26] to provide sufficient material for lab-scale studies. The current purification approaches include polymer wrapping,[15-17] non-covalent functionalization,[18-21] DNA and peptide mediated isolation,[22-25] and dispersion in aqueous solution via ionic surfactants.[26] In addition to the use of surfactants, these methods often rely on sonication, which has been shown to result in damage to the BNNTs.[27] Another attractive purification route

is simple chemical purification using acids and solvents; however, this is difficult due to the chemical similarity between the h-BN impurities and BNNTs. These approaches are difficult to scale up to provide sufficient material for macroscopic articles and composites of pristine BNNTs.

Here, we demonstrate purification and assembly of BNNTs into macroscale articles via solution processing with chlorosulfonic acid (CSA) as a solvent. A recent study indicated that CSA acts as a true solvent for BNNTs.[28] In the current study, the preferential solubility of BNNTs compared to h-BN and other byproducts is used to extract BNNTs without surfactants or sonication. Furthermore, we show the formation of sub-micron BNNT layer films, millimeter thick mats, and centimeter scale BNNT foams through the use of CSA.

All the BNNTs used in this report were synthesized by the high temperature high pressure process and supplied by NASA.[12] Our initial analysis by high-resolution scanning electron microscopy (HR-SEM), x-ray photoelectron spectroscopy (XPS), and x-ray diffraction (XRD) (presented in the supporting information) indicated that the starting material contains elemental boron, h-BN, and boron oxide (B_2O_3) in addition to BNNTs.

Infrared spectroscopy (ATR IR), x-ray photoelectron spectroscopy (XPS), and thermogravimetric analysis (TGA) were used to determine any possible reactions of CSA with BNNTs (details in supplementary information). As-synthesized BNNTs were mixed with CSA (Sigma Aldrich) at 0.7 wt% to form a gray slurry. The slurry was then filtered through a 25 mm diameter, 20 nm pore-size alumina filter (Whatman Anodisc 25), and formed a wet disc. Chloroform (Sigma Aldrich) was added to precipitate the BNNT solids and remove CSA, followed by washing with ethyl alcohol (Fisher Scientific) and water to remove chloroform, sulfuric acid, hydrochloric acid, and other CSA-chloroform reaction byproducts prior to drying in vacuum at 35 °C for 48 hours. The

ATR IR data from the CSA-treated BNNT material showed some broadening and a small shift of the B-N peaks with no new spectral features. Although XPS indicated that residual sulfur and chlorine are present in the CSA-treated BNNT material, this is due to residual acid. The absence of new spectral features attributable to BNNT functionalization indicates that no permanent chemical reactions between BNNTs and CSA occurred, in agreement with previous electron energy loss spectroscopy.[28] In addition to permitting analysis of the BNNT-CSA interactions, this process also illustrates one route to form structurally stable BNNT mats.

The extraction of BNNTs was performed by centrifugation. BNNTs were mixed with CSA at 100 ppm (by mass) in a speed-mixer (FlackTek DAC600.1FVZ) at 3250 rpm for 1 hour to form a beige-colored BNNT-CSA slurry. The BNNT-CSA slurry was centrifuged in a Sorvall Legend X1 at 3500 x g and separated into two phases with a clear, golden-colored solution supernatant, similar to h-BN dispersed in CSA.[29, 30] The clear supernatant was separated using a Pasteur pipette, then filtered to form sub-micron thin films.

Sub-micron thin films were prepared by filtering the supernatant using a 20 nm pore size alumina filter paper and transferred onto substrates (borosilicate glass slides and perfluoroalkoxy alkane (PFA) films) by floating the film in water.[31, 32] Thin films with thickness ~10 nm (maximum height in cross-section SEM) were deposited on a glass microscope slide (**Figure 1A** inset). Characterization by HR-SEM was carried out after 24 hours of air drying (**Figure 1A**).

Thicker films (~500 nm as estimated by cross-section SEM) were prepared by filtering supernatants from two batches of extracted material (150 mg BNNTs dissolved in 10 mL CSA each). The thicker films were transferred to PFA substrates (McMaster-Carr) and later peeled off with tweezers (**Figure 1B** inset), indicating that BNNTs do not physisorb to PFA. Unlike the thin

films, the thicker films were self-supporting; to our knowledge, this is the first demonstration of a self-standing sub-micron macroscopic artifact composed of BNNTs in the absence of a polymer matrix or binders.
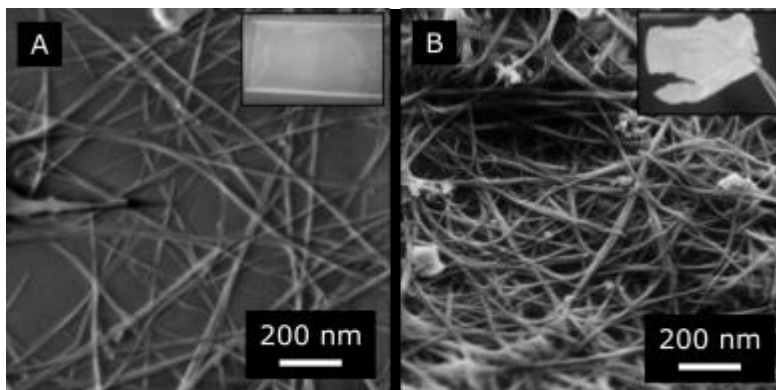
Figure 1. A. HR-SEM of a thin film of BNNTs from the supernatant after centrifugation. **B.** HR-SEM of the self-supporting film. Insets show the macroscopic appearance of the material imaged by HR-SEM.

Figure 1A shows a HR-SEM (Zeiss Ultra Plus SEM; 0.7-2 kV acceleration voltage, 2.9-3.3 mm separation distance) image of the thin film coated on a glass substrate. A low accelerating voltage of 1.00 kV was used to minimize charging on the insulating sample with no metal coating. An increase in the ratio of nanotubes to non-nanotube structures was observed compared to images of the as-synthesized material (see supporting information), and indicated that the preferential dissolution of nanotubes in CSA may be used to purify the as-synthesized material. **Figure 1B** is a HR-SEM image of the freestanding thicker film showing an interconnected network of BNNT bundles with few non-nanotube structures. This interconnected structure provides the necessary mechanical support for the thin film to resist fracture under its own weight.

Backscattered SEM images (see supplementary information) do not indicate a significant variation in density between the BNNTs and non-nanotube structures that remain in the supernatant. Since

6

Smith *et al.* reported that the BNNTs formed by the HTP process has a B:N ratio of 1,[12] it is probable that the non-nanotube structures observed are impurities such as h-BN, boron, or B_2O_3. These non-nanotube structures are likely present in the supernatant because they are chemically bonded to BNNTs, permitting them to remain suspended in CSA post-centrifugation. Chemical bonding between BNNTs and the impurities is expected since the current proposed model for BNNT growth in the HTP synthesis begins with the condensation of boron droplets, which then react with atomic nitrogen in high pressure to form BNNTs on the droplet surfaces.[12] This synthesis mechanism explains why star-shaped structures can be seen in the supernatant, with non-nanotube impurities holding fibrils together at a common hub (**Figure 1A**).

The remaining material from the extraction process was gradually quenched in excess water, solids filtered, then dried in an oven (Lindberg / Blue M Gravity Oven) at 150 °C for 48 hours. Analysis on the precipitate (supporting information) indicated the presence of elemental boron, h-BN, and B_2O_3 with a small percentage of BNNTs. This indicates that although the extraction process does not remove all BNNTs, it will sufficiently remove all individualized BNNTs. It is expected that the BNNTs not dissolved in CSA are bonded to non-nanotubes.

Since as-synthesized BNNTs form stable dispersions in CSA, methods used for solution processing CNTs[33-37] may also be applied to BNNTs. As a demonstration, a 2000 ppm mass concentration of BNNT in CSA slurry was poured into 1 cm^3 steel mesh cages (McMaster-Carr) wrapped with Teflon tape (McMaster-Carr) and coagulated in cold ether (Fisher Scientific). The gels shrank to ~0.5 cm^3 upon coagulation (**Figure 2**). This process resembles the injection molding of CNTs as demonstrated by Hsu et al.[38] Similar processes may be used to prepare high-surface-area BNNT foams for a variety of applications.
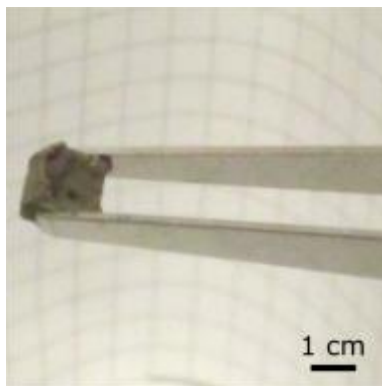
Figure 2. BNNT foam (0.5 cm^3) foam fabricated by coagulating a BNNT/CSA solution in cold diethyl ether.

In conclusion, solubility-driven separation was used to extract BNNTs from byproducts in CSA. ATR IR showed that CSA does not chemically functionalize or react with BNNTs at room temperature and pressure. The preferential solubility of BNNTs in CSA permits scaled solution processing to extract BNNTs. The solution can be filtered and collected on various surfaces to form thermally conductive, chemically resistant thin films that can protect a substrate from extreme heat and corrosion. In addition, the suspension of as-produced BNNT material in CSA provides the first route for molding BNNT foams into any desired shape. The mats and films produced herein may be used for low-density thermal protection articles capable of withstanding high temperatures in an oxidizing environment.

ASSOCIATED CONTENT

The following files are available free of charge.

Spectroscopy of precipitates. Backscattered SEM, XPS, XRD, ATR IR, TGA, and DSC on the processed material (PDF).

AUTHOR INFORMATION

Corresponding Author

‡Matteo Pasquali (mp@rice.edu)

Department of Chemical and Biomolecular Engineering and Department of Chemistry

Rice University

6100 Main Street, MS 369

Houston, TX 77005, USA

Present Addresses

†Dr. Mohammed Adnan now with Abu Dhabi Financial Group, Abu Dhabi, UAE.

Author Contributions

The manuscript was written through contributions of all authors. All authors have given approval to the final version of the manuscript.

Notes

HR-SEM imaging was performed at the Laboratory for Electron Microscopy of Soft Matter, supported by the Technion Russell Berrie Nanotechnology Institute (RBNI).

ACKNOWLEDGMENT

ABBREVIATIONS

BNNT, boron nitride nanotube; h-BN, hexagonal boron nitride; CNT, carbon nanotubes; HTP, high temperature-pressure; CSA, chlorosulfonic acid; B_2O_3, boron oxide; ATR IR, attenuated total reflectance infrared spectroscopy; PFA, perfluoroalkoxy alkane; HR-SEM, high resolution scanning electron microscopy; XPS, x-ray photoelectron spectroscopy; XRD, x-ray diffraction

REFERENCES

1. Arenal, R.; Wang, M. S.; Xu, Z.; Loiseau, A.; Golberg, D. *Nanotechnology* **2011,** 22, (26), 6.
2. Chang, C. W.; Fennimore, A. M.; Afanasiev, A.; Okawa, D.; Ikuno, T.; Garcia, H.; Li, D. Y.; Majumdar, A.; Zettl, A. *Physical Review Letters* **2006,** 97, (8), 4.
3. Golberg, D.; Bando, Y.; Huang, Y.; Terao, T.; Mitome, M.; Tang, C. C.; Zhi, C. Y. *ACS Nano* **2010,** 4, (6), 2979-2993.
4. Chen, Y.; Zou, J.; Campbell, S. J.; Le Caer, G. *Applied Physics Letters* **2004,** 84, (13), 2430-2432.
5. Nakhmanson, S. M.; Calzolari, A.; Meunier, V.; Bernholc, J.; Nardelli, M. B. *Physical Review B* **2003,** 67, (23), 5.
6. Gao, R.; Yin, L. W.; Wang, C. X.; Qi, Y. X.; Lun, N.; Zhang, L. Y.; Liu, Y. X.; Kang, L.; Wang, X. F. *Journal of Physical Chemistry C* **2009,** 113, (34), 15160-15165.
7. Daniel, A.; Badhe, Y.; Srikanth, I.; Gokhale, S.; Balasubramanian, K. *Industrial & Engineering Chemistry Research* **2016,** 55, (40), 10645-10655.
8. Tiano, A. L.; Park, C.; Lee, J. W.; Luong, H. H.; Gibbons, L. J.; Chu, S.-H.; Applin, S.; Gnoffo, P.; Lowther, S.; Kim, H. J.; Danehy, P. M.; Inman, J. A.; Jones, S. B.; Kang, J. H.; Sauti, G.; Thibeault, S. A.; Yamakov, V.; Wise, K. E.; Su, J.; Fay, C. C. *Proc. SPIE* **2014,** 9060, 906006-906006-19.
9. Pakdel, A.; Zhi, C. Y.; Bando, Y.; Golberg, D. *Materials Today* **2012,** 15, (6), 256-265.
10. Chopra, N. G.; Luyken, R. J.; Cherrey, K.; Crespi, V. H.; Cohen, M. L.; Louie, S. G.; Zettl, A. *Science* **1995,** 269, (5226), 966-967.
11. Lee, C. H.; Bhandari, S.; Tiwari, B.; Yapici, N.; Zhang, D. Y.; Yap, Y. K. *Molecules* **2016,** 21, (7), 19.

12. Smith, M. W.; Jordan, K. C.; Park, C.; Kim, J. W.; Lillehei, P. T.; Crooks, R.; Harrison, J. S. *Nanotechnology* **2009,** 20, (50), 6.

13. Kim, K. S.; Kingston, C. T.; Hrdina, A.; Jakubinek, M. B.; Guan, J. W.; Plunkett, M.; Simard, B. *ACS Nano* **2014,** 8, (6), 6211-6220.

14. Fathalizadeh, A.; Pham, T.; Mickelson, W.; Zettl, A. *Nano Letters* **2014,** 14, (8), 4881-4886.

15. Zhi, C. Y.; Bando, Y.; Tang, C. C.; Xie, R. G.; Sekiguchi, T.; Golberg, D. *Journal of the American Chemical Society* **2005,** 127, (46), 15996-15997.

16. Choi, J. H.; Kim, J.; Seo, D.; Seo, Y. S. *Materials Research Bulletin* **2013,** 48, (3), 1197-1203.

17. Zhi, C. Y.; Bando, Y.; Tang, C. C.; Honda, S.; Sato, K.; Kuwahara, H.; Golberg, D. *Angewandte Chemie-International Edition* **2005,** 44, (48), 7929-7932.

18. Xie, S. Y.; Wang, W.; Fernando, K. A. S.; Wang, X.; Lin, Y.; Sun, Y. P. *Chemical Communications* **2005**, (29), 3670-3672.

19. Kim, D.; Sawada, T.; Zhi, C. Y.; Bando, Y.; Golberg, D.; Serizawa, T. *Journal of Nanoscience and Nanotechnology* **2014,** 14, (4), 3028-3033.

20. Wang, W. L.; Bando, Y.; Zhi, C. Y.; Fu, W. Y.; Wang, E. G.; Golberg, D. *Journal of the American Chemical Society* **2008,** 130, (26), 8144.

21. Velayudham, S.; Lee, C. H.; Xie, M.; Blair, D.; Bauman, N.; Yap, Y. K.; Green, S. A.; Liu, H. Y. *ACS Applied Materials & Interfaces* **2010,** 2, (1), 104-110.

22. Zhi, C.; Bando, Y.; Wang, W.; Tang, C.; Kuwahara, H.; Golberg, D. *Chemistry-an Asian Journal* **2007,** 2, (12), 1581-1585.

23. Gao, Z. H.; Zhi, C. Y.; Bando, Y.; Golberg, D.; Serizawa, T. *Journal of the American Chemical Society* **2010,** 132, (14), 4976.

24. Ansari, R.; Ajori, S.; Ameri, A. *Applied Surface Science* **2016,** 366, 233-244.

25. Lee, C. H.; Zhang, D. Y.; Yap, Y. K. *Journal of Physical Chemistry C* **2012,** 116, (2), 1798-1804.

26. Yu, J.; Chen, Y.; Cheng, B. M. *Solid State Communications* **2009,** 149, (19-20), 763-766.

27. Liao, Y.; Chen, Z.; Connell, J. W.; Fay, C. C.; Park, C.; Kim, J.-W.; Lin, Y. *Advanced Functional Materials* **2014,** 24, (28), 4497-4506.

28. Kleinerman, O.; Mohammed, A.; Marincel, D. M.; Ma, A. W. K.; Bengio, A.; Park, C.; Chu, S.-H.; Pasquali, M.; Talmon, Y. *Unpublished Experiments*.

29. Jasuja, K. Designing nanoscale constructs from atomic thin sheets of graphene, boron nitride and gold nanoparticles for advanced material applications. Kansas State University, 2011.

30. Morishita, T.; Okamoto, H. *ACS Applied Materials & Interfaces* **2016,** 8, (40), 27064-27073.

31. Hecht, D. S.; Heintz, A. M.; Lee, R.; Hu, L. B.; Moore, B.; Cucksey, C.; Risser, S. *Nanotechnology* **2011,** 22, (7), 5.

32. Wu, Z. C.; Chen, Z. H.; Du, X.; Logan, J. M.; Sippel, J.; Nikolou, M.; Kamaras, K.; Reynolds, J. R.; Tanner, D. B.; Hebard, A. F.; Rinzler, A. G. *Science* **2004,** 305, (5688), 1273-1276.

33. Vitale, F.; Summerson, S. R.; Aazhang, B.; Kemere, C.; Pasquali, M. *ACS Nano* **2015,** 9, (4), 4465-4474.

34. Mirri, F.; Ma, A. W. K.; Hsu, T. T.; Behabtu, N.; Eichmann, S. L.; Young, C. C.; Tsentalovich, D. E.; Pasquali, M. *ACS Nano* **2012,** 6, (11), 9737-9744.

35. Pasquali, M.; Whiting, T. Y. T. H.; Mirri, F.; Whiting, B. T., Fabrication of carbon foams through solution processing in superacids. US 20140141224, 2014.

36. Behabtu, N.; Lomeda, J. R.; Green, M. J.; Higginbotham, A. L.; Sinitskii, A.; Kosynkin, D. V.; Tsentalovich, D.; Parra-Vasquez, A. N. G.; Schmidt, J.; Kesselman, E.; Cohen, Y.; Talmon, Y.; Tour, J. M.; Pasquali, M. *Nature Nanotechnology* **2010,** 5, (6), 406-411.

37. Bengio, E. A.; Tsentalovich, D. E.; Behabtu, N.; Kleinerman, O.; Kesselman, E.; Schmidt, J.; Talmon, Y.; Pasquali, M. *ACS Applied Materials & Interfaces* **2014,** 6, (9), 6139-6146.

38. Hsu, T. T.; Whiting, B. T.; Mirri, F.; Williams, S. M.; Yu, M.; Ganguli, S.; Amama, P. B.; Zhao, W.; Rajukumar, L. P.; Cheng, G.; Walker, A. R. H.; Terrones, M.; Suhr, J.; Maruyama, B.; Roy, A. K.; Pasquali, M. *Unpublished Experiments*.

Extraction of boron nitride nanotubes and fabrication of macroscopic articles using chlorosulfonic acid

Supporting Information: Spectroscopy of Precipitates

1   HR-SEM of As-synthesized Material

High resolution SEM of the BNNTs as-synthesized and after CSA extraction are shown in **Figure S3**. A higher percentage of the objects observed are fibrils after extraction compared to before. Star-shaped structures can be seen in the extracted material, indicating that impurities attached to BNNTs are not fully removed.
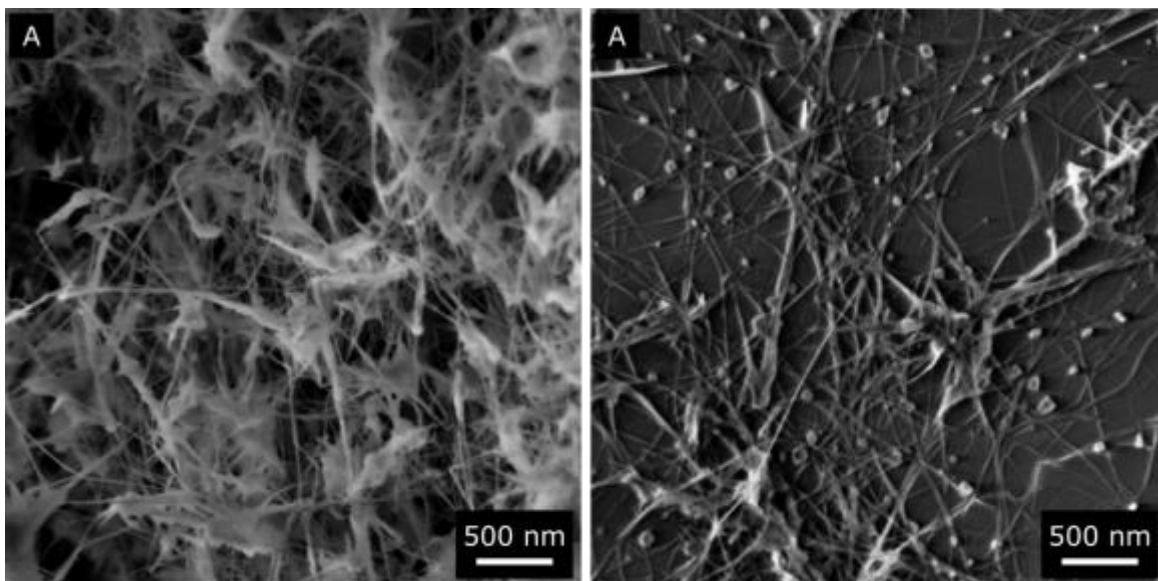

Figure S3: HR-SEM of BNNTs (a) before and (b) after CSA extraction. Note that the small particles are silicon dioxide contaminants from cutting the glass slide after the BNNTs were collected.

# 2 X-Ray Photoelectron Spectroscopy (XPS)

2.1 Survey Scans

XPS survey scans show approximate elemental compositions of the as-synthesized material and the precipitates using a pass energy of 26 eV (**Figure S4**). The as-synthesized BNNTs have boron, nitrogen, oxygen, and carbon at concentrations of 48.8 at.%, 48.1 at.%, 2.4 at.%, and 0.7 at.%, respectively. Adventitious oxygen and carbon are likely contaminants on the sample surface and in the XPS stage. After exposure to CSA followed by direct quenching in chloroform and washing in isopropanol and water (i.e. no centrifugation), the material consisted of approximately 35 at.% of boron and nitrogen in a 1:1 ratio. However, approximately 21 at.% oxygen along with 10 at.% adventitious carbon was detectable. The remaining 2 at.% was composed of sulfuric acid.
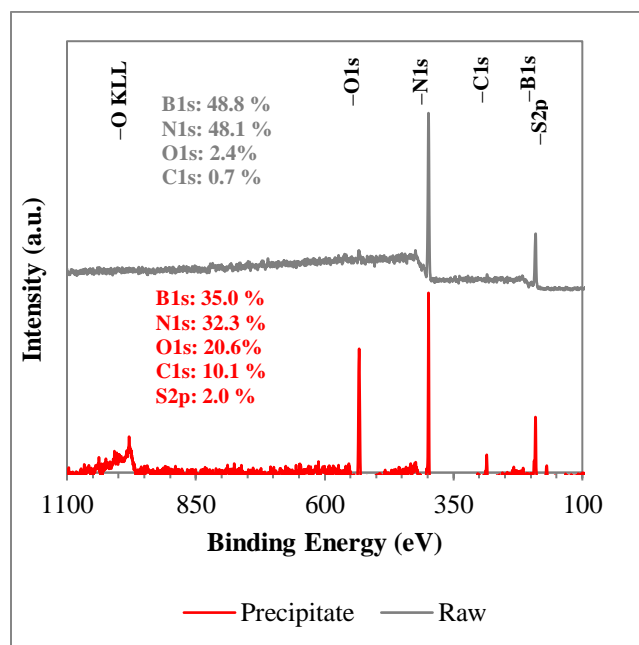

Figure S4. Survey scans of as-synthesized BNNTs and precipitates between 100 – 1100 eV showing presence of sulfur, boron, carbon, nitrogen, and oxygen before (top, gray) and after (bottom, red) exposure to CSA.

2.2 Deconvolution on As-Synthesized Material

Deconvolution of the scans indicates the presence of elemental boron, and $B_xN_yO_z$ species as the chief impurities present in as-synthesized BNNTs (Figure S5). Presence of elemental boron, BN and $B_xN_yO_z$, and B_2O_3 species were observed at binding energies of 187.7 eV, 190.6 eV, 192.8 eV, and 193.4 eV, respectively, for B1s signals. N1s signals also confirm the presence of BN at 398.3 eV, $B_xN_yO_z$ species at 400.3 eV, along with presence of possible contamination at 395.4 eV. XPS peaks obtained due to oxygen and carbon were too noisy to be delineated.

14

B1s
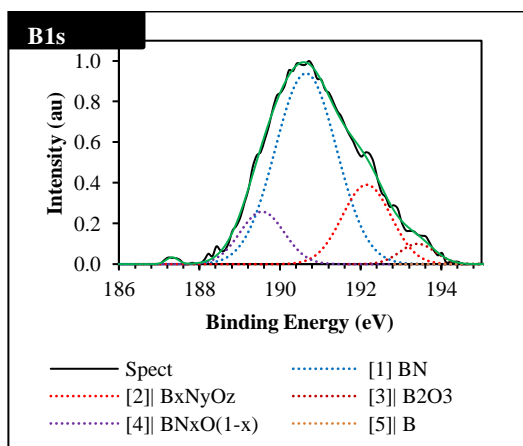
[1] BN
Position: 190.62 eV
Height: 0.3
FWHM: 2.0 eV
[2] $B_xN_yO_z$
Position: 192.82 eV
Height: 0.2
FWHM: 1.6 eV
[3] B_2O_3
Position: 193.4 eV
Height: 0.2
FWHM: 1.3 eV
[4] $BN_xO_{(1-x)}$
Position: 189.5 eV
Height: 0.2
FWHM: 1.5 eV
[5] B
Position: 187.3 eV
Height: 2E-5
FWHM: 0.5 eV

χ^2: 0.262

N1s
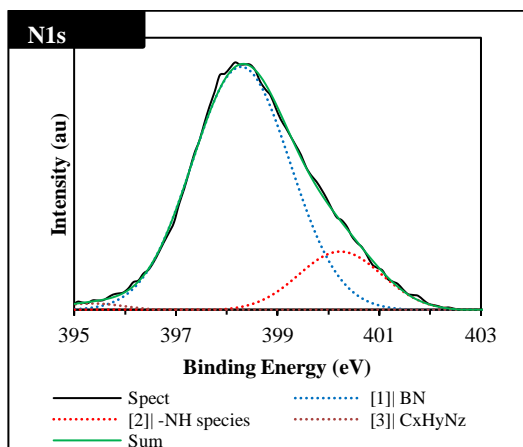
[1] BN
Position: 398.3 eV
Height: 0.5
FWHM: 2.5 eV
[2] $B_xN_yO_z$
Position: 400.3 eV
Height: 0.3
FWHM: 2.1 eV
[3] $C_xH_yN_z$ (contamination)
Pos: 395.4 eV
Height: 0.2
FWHM: 1.4 eV

χ^2: 0.048

Figure S5. Deconvolution of B1s and N1s spectra of as-synthesized BNNTs showing the presence of elemental boron, $B_xN_xO_y$ species, and BN species.
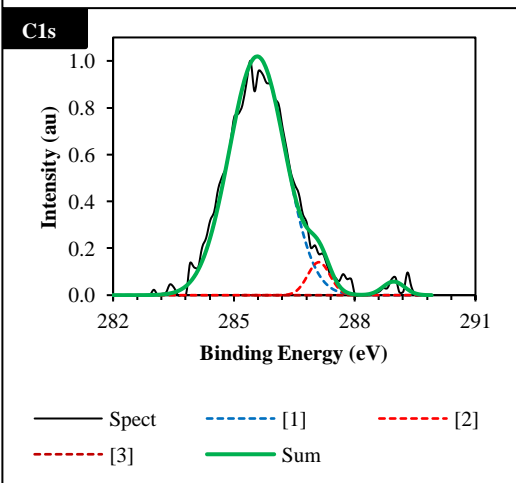
2.3   Deconvolution on CSA Processed BNNTs

Deconvolutions of the oxygen, carbon, sulfur, boron, and nitrogen peaks for the pellet after centrifugation and quenching with water are shown by **Figure S6**. Full deconvolution fit data is provided in the figure.
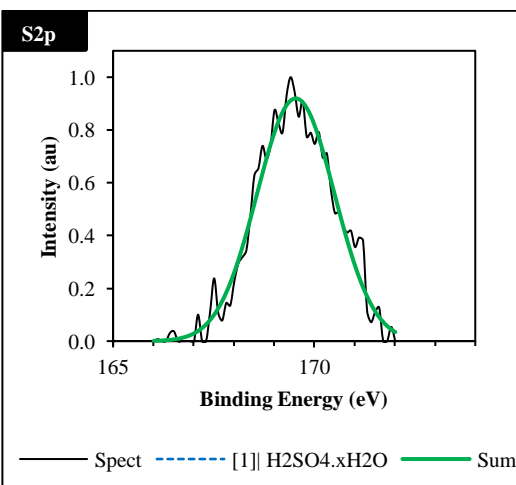
O1s
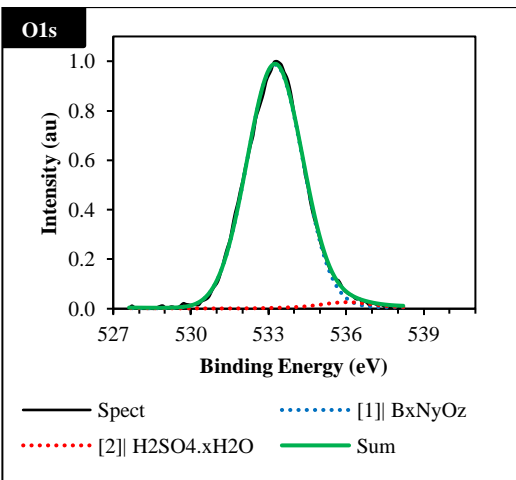
[1] $B_xN_yO_z$
Position: 533.2 eV
Height: 0.7
FWHM: 2.8 eV
[2] $H_2SO_4*2H_2O$
Position: 536.0 eV
Height: 0.3
FWHM: 2.7 eV

χ^2: **0.234**

C1s

[1]
Position: 285.6 eV
Height: 0.4
FWHM: 1.8 eV
[2]
Position: 287.1 eV
Height: 0.3
FWHM: 0.9 eV
[3]
Position: 289.0 eV
Height: 0.3
FWHM: 1.1 eV

χ^2: **2.482**

S2p

Position: 169.5 eV
FWHM: 2.8 eV

χ^2: **2.039**

B1s
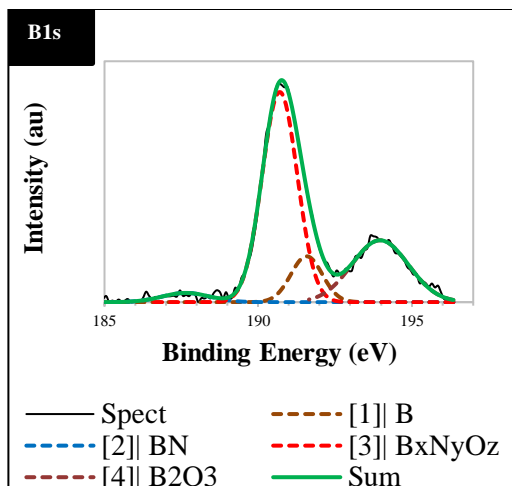
[1] B
Position: 187.7 eV
Height: 0.03
FWHM: 1.8 eV
[2] BN
Position: 190.7 eV
Height: 0.6
FWHM: 1.3 eV
[3] $B_xN_yO_z$
Position: 191.6 eV
Height: 0.1
FWHM: 1.2 eV
[4] B_2O_3
Position: 194.0 eV
Height: 0.2
FWHM: 2.2 eV

χ^2: 0.269

N1s
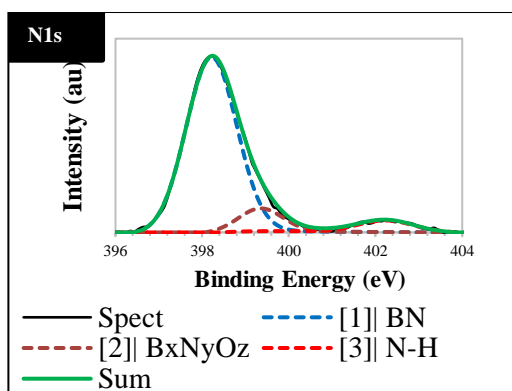
[1] BN
Position: 398.2 eV
Height 0.5 eV
FWHM: 1.6 eV
[2] $B_xN_yO_z$
Position: 402.2 eV
Height: 0.2
FWHM: 1.8 eV
[3] N-H
Position: 399.3 eV
Height: 0.3
FWHM: 1.4 eV

χ^2: 0.206

Figure S6. XPS on BNNT precipitates showing B1s, N1s, O1s, S1s, and C1s binding energies.

17

Data on the XPS deconvolutions for as-synthesized BNNTs and after quenching from CSA is shown in **Table S1** to assist in comparison for the reader.

Table S1: Peak-fit deconvolution of XPS peaks for as-produced BNNT and CSA treated BNNT solids.

B(1s)	BNNT	CSA treated BNNT	N(1s)	BNNT	CSA treated BNNT	O(1s)	BNNT	CSA treated BNNT	C(1s)	BNNT	CSA treated BNNT	S(2p)	BNNT	CSA treated BNNT
BN			**BN**						**[1]**			**[1]**		
Position	190.6	190.7		398.3	398.2		-	-		-	285.6		-	169.5
Height	0.3	0.6		0.5	0.5		-	-		-	0.4		-	-
FWHM	2	1.3		2.5	1.6		-	-		-	1.8		-	2.8
$B_xN_yO_z$			**$B_xN_yO_z$**			**$B_xN_yO_z$**			**[2]**					
Position	192.82	191.6		400.3	402.2		-	533.2		-	287.1		-	-
Height	0.2	0.1		0.3	0.2		-	0.7		-	0.3		-	-
FWHM	1.6	1.2		2.1	1.8		-	2.8		-	0.9		-	-
B_2O_3			**$C_xH_yN_z$ (contamination)**			**$H_2SO_4*2H_2O$**			**[3]**					
Position	193.4	194		395.4	-		-	536		-	289		-	-
Height	0.2	0.2		0.2	-		-	0.3		-	0.3		-	-
FWHM	1.3	2.2		1.4	-		-	2.7		-	1.1		-	-
$BN_xO_{(1-x)}$			**N-H**											
Position	189.5	-		-	399.3		-	-		-	-		-	-
Height	0.2	-		-	0.3		-	-		-	-		-	-
FWHM	1.5	-		-	1.4		-	-		-	-		-	-
[5] B														
Position	187.3	187.7		-	-		-	-		-	-		-	-
Height	2E-05	0.03		-	-		-	-		-	-		-	-
FWHM	0.5	1.8		-	-		-	-		-	-		-	-
χ^2	0.262	0.269		0.048	0.206			0.234			2.482			2.039

3 X-Ray Diffraction

X-Ray Diffraction (XRD) on precipitates of as-synthesized BNNTs processed with CSA and quenched in water was conducted on a Rigaku D/Max Ultima II equipped with a Cu-K$_\alpha$ radiation source to characterize the phases present in the sample. A mortar and pestle was used to grind the solid samples into powder that was then placed in a cavity backfill powder diffraction holder for XRD analysis.
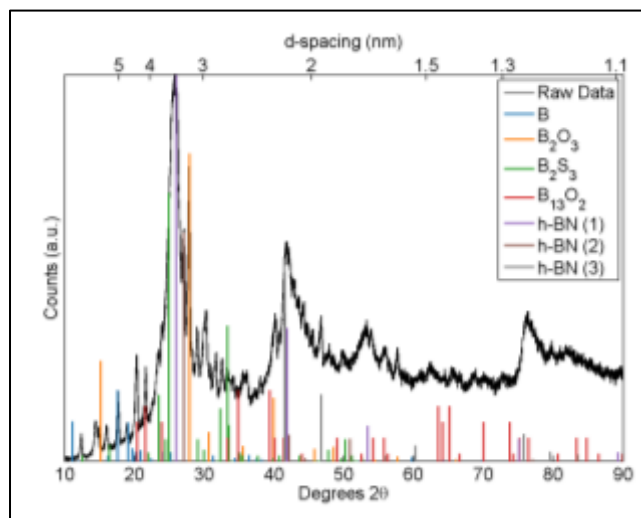
Figure S7. XRD on precipitate from BNNT/CSA solution. Peaks of elemental boron are marked with blue line, B_2O_3 with orange line, B_2S_3 with green line, $B_{13}O_2$ marked with red line. h-BN with different interlayer spacings are marked with purple, brown and grey lines.

In order to purify BNNTs from non-nanotube structures, it is imperative to analyze the nature of the by-products. The results from XRD on precipitates are shown in **Figure S7**. It was found that h-BN with a range of interplanar spacing is present in the sample, as shown by multiple peaks near 27° 2θ. Additionally, elemental boron is observed. Peaks corresponding to boron-sulfur compounds can be observed in the sample, which may be due to elemental boron or boric acid in the as-synthesized material reacting with CSA to produce boron sulfonic acid[1] which then degrades to boron sulfide. Similarly, boron oxide may develop due to extended exposure to atmosphere or washing the precipitate with water after saturation with CSA. XRD analysis is unable to differentiate BNNTs from h-BN as both polymorphs have the same diffraction pattern. It is observed that phases in as-synthesized BNNTs having poor solubility in CSA precipitated and primarily consisted of elemental boron, h-BN, and BNNTs filled with CSA.

4 Fourier Transform Infrared Spectroscopy

Comparison between the chemical structure of the as-synthesized BNNTs before and after treatment with CSA was observed by attenuated total reflectance infrared spectroscopy (ATR IR, Nicolet Nexus 670 FTIR with a Smart iTR Attenuated Total Reflectance Sampling Accessory) (**Figure S8**). A sharp peak appearing between 775 cm^{-1} to 819 cm^{-1} corresponds to the B-N-B

radial buckling (R) mode. The sharp peak between 1324 cm^{-1} and 1361 cm^{-1} (at which the spectra were normalized) corresponds to the h-BN in-plane stretching and BNNT stretching along the tube length (L). A shoulder observed around 1480 cm^{-1} correspond to the tangential (T) B-N in-plane stretching around the tube circumference. The broad T mode vibrational band is attributed to the polydispersity in BNNT radii and chirality.[2] An additional peak of lower intensity around 3250 cm^{-1} appears due to stretching of O-H bonds of residual moisture.

After exposure to CSA, the longitudinal peak shifts from 1361 to 1324 cm^{-1} and broadens. Due to the absence of additional peaks, it is inferred that no permanent chemical reaction between BNNTs and CSA had occurred.
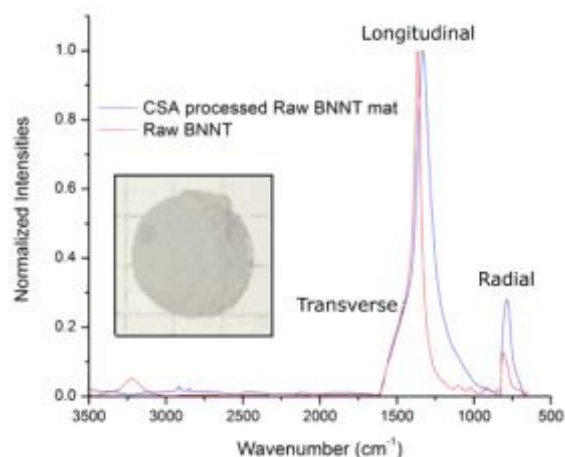
Figure S8. ATR IR spectroscopy of as-synthesized BNNTs and CSA processed BNNTs. The inset shows the mat that was fabricated via filtration from a CSA solution and used for ATR IR characterization. Each square of the grid in the image of the inset represents 1 cm.

5 Thermogravimetric Analysis with Differential Scanning Calorimetry
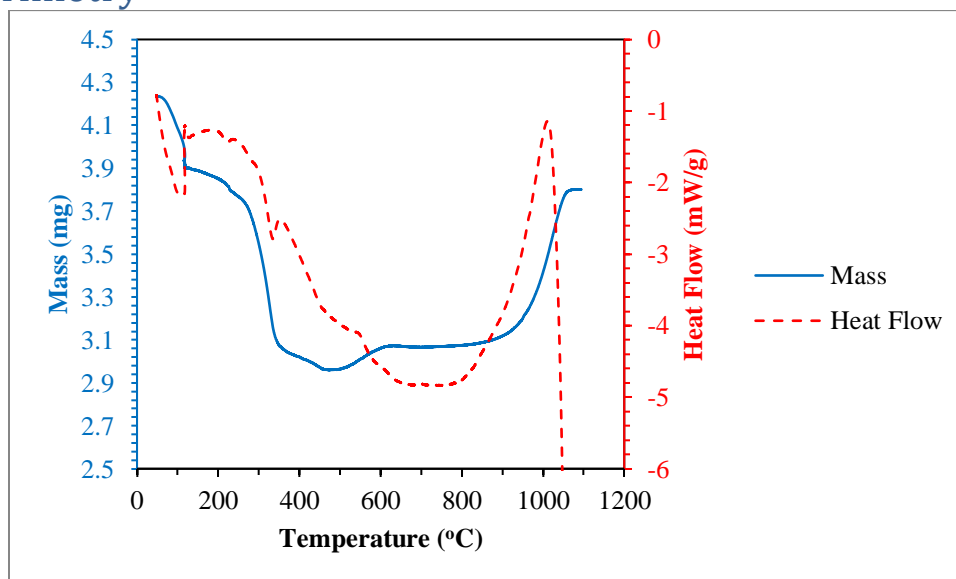
Figure S9. TGA and DSC analysis of precipitates. Solid line represents the TGA graph, while the dotted line represents the heat flow.

Thermogravimetric analysis (TGA) and differential scanning colorimetry (DSC) scans between 25°C to 1100°C on 4.24 mg of precipitates exposed to a dry air flow at 100 ml/hr are shown in **Figure S9**. The DSC curves were used to find the onset points and nature of the reaction. A description of the reactions with corresponding change in mass is provided in **Table S2**. Evaporation of water at 100°C is marked by the endothermic DSC profile, and loss of 7.9% of the mass. Further loss of 3.2% mass at 223°C, 17.1% at 335°C and 1.9% at 455°C. Mass gain at 545°C by 2.5% is most likely oxidation of boron with the dramatic increase at 1010°C showing high temperature stability of the BN polymorphs. The unchanged mass after 1100°C is assumed to be boron oxide.

Table S2. Reactions and corresponding mass changes from the TGA/DSC of precipitates between 25 °C to 1100 °C with dry air flowing at 100 mL/min

Temperature (°C)	Mass Change (%)
100	-7.9
223	-3.2
335	-17.1
455	-1.9

545	+2.5
1010	+17.3

6 Backscattered SEM Images

Backscattered SEM image of the thin film fabricated from the supernatant is shown in **Figure S10**. Particles with higher density or higher Z (marked with arrows) tend to appear brighter than the BNNT fibrils. These particles are likely silicon oxide that originate from cutting the glass slide after collecting the BNNTs. Other non-BNNT material shows a similar contrast in backscatter to BNNTs.
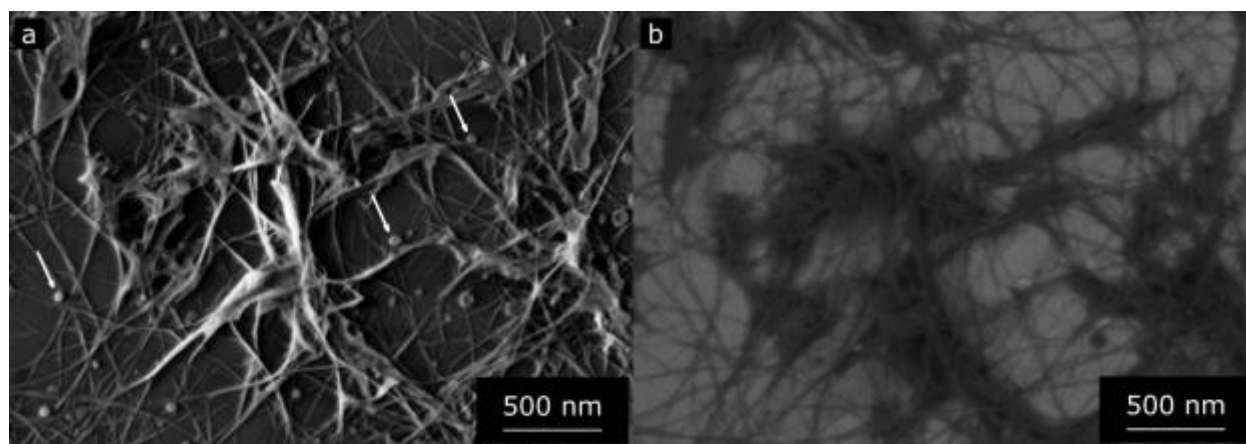
Figure S10. (a) Secondary and (b) backscattered images of the thin film deposited on the glass slide. Arrows show particles that are brighter in backscatter than BNNTs, implying a higher electron density, likely silicon oxide from the glass slide.

7 Bibliography

1. Kiasat, A. R.; Fallah-Mehrjardi, M., B(HSO4)3: a novel and efficient solid acid catalyst for the regioselective conversion of epoxides to thiocyanohydrins under solvent-free conditions. *Journal of the Brazilian Chemical Society* **2008,** *19*, 1595-1599.

2. Wirtz, L.; Rubio, A.; de la Concha, R. A.; Loiseau, A., Ab initio calculations of the lattice dynamics of boron nitride nanotubes. *Physical Review B* **2003,** *68* (4), 13.